# Impact of Climate Change on New York City's Coastal Flood Hazard: Increasing Flood Heights from the Pre-Industrial to 2300 CE

Andra J. Garner[a*], Michael E. Mann[b,c], Kerry A. Emanuel[d], Robert E. Kopp[e], Ning Lin[f], Richard B. Alley[g], Benjamin P. Horton[a,h,i], Robert M. DeConto[j], Jeffrey P. Donnelly[k], David Pollard[c]

*Corresponding Author:*
Andra J. Garner
Department of Marine and Coastal Sciences
Rutgers University
71 Dudley Road
New Brunswick, NJ 08901
848-932-3482
ajgarner@marine.rutgers.edu

[a]*Department of Marine and Coastal Sciences and Institute of Earth, Ocean, and Atmospheric Sciences, Rutgers University, New Brunswick, NJ 08901*
[b]*Department of Meteorology and Atmospheric Science, The Pennsylvania State University, University Park, PA 16802*
[c]*Earth and Environmental Systems Institute, The Pennsylvania State University, University Park, PA 16802*
[d]*Department of Earth, Atmospheric, and Planetary Sciences, Program in Atmospheres, Oceans, and Climate, Massachusetts Institute of Technology, Cambridge, MA 02913*
[e]*Department of Earth and Planetary Sciences and Institute of Earth, Ocean, and Atmospheric Sciences, Rutgers University, Piscataway, NJ 08854*
[f]*Department of Civil and Environmental Engineering, Princeton University, Princeton, NJ 08544*
[g]*Department of Geosciences, The Pennsylvania State University, University Park, PA 16802*
[h] *Asian School of the Environment, Nanyang Technological University 639798, Singapore.*
[i]*Earth Observatory of Singapore, Nanyang Technological University 639798, Singapore*
[j]*Department of Geosciences, University of Massachusetts—Amherst, Amherst, MA 01003*
[k]*Department of Geology and Geophysics, Woods Hole Oceanographic Institution, Woods Hole, MA 02543*

*Classification:* PHYSICAL SCIENCES: Earth, Atmospheric, and Planetary Sciences

*Short title for mobile devices and RSS feeds:* Increased NYC flood hazard: Pre-Industrial to 2300

*Keywords:* Tropical Cyclones, Flood Height, Storm Surge, New York City, Sea-level Rise, Hurricane, Coastal Flooding, Storm Tracks

[*] *Corresponding author e-mail address:* ajgarner@marine.rutgers.edu

# Abstract

The flood hazard in New York City depends on both storm surges and rising sea levels. We combine modeled storm surges with probabilistic sea-level rise projections to assess future coastal inundation in New York City from the pre-industrial era through 2300 CE. The storm surges are derived from large sets of synthetic tropical cyclones, downscaled from RCP8.5 simulations from three CMIP5 models. The sea-level rise projections account for potential, partial collapse of the Antarctic Ice Sheet in assessing future coastal inundation. CMIP5 models indicate that there will be minimal change in storm-surge heights from 2010 to 2100 or 2300, because the predicted strengthening of the strongest storms will be compensated by storm tracks moving offshore at the latitude of New York City. However, projected sea-level rise causes overall flood heights associated with tropical cyclones in New York City in coming centuries to increase greatly compared to pre-industrial or modern flood heights. We find that the 1-in-500-year flood event increases from 3.4 m above mean tidal level during 1970-2005 to 4.0 – 5.1 m above mean tidal level by 2080-2100, and ranges from 5.0 – 15.4 m above mean tidal level by 2280-2300. Further, we find that the return period of a 2.25 m flood has decreased from ~500 years prior to 1800 to ~25 years during 1970-2005, and further decreases to ~5 years by 2030 – 2045 in 95% of our simulations. The 2.25 m flood height is permanently exceeded by 2280 – 2300 for scenarios that include Antarctica's potential partial collapse.

## Significance Statement

We combine downscaled tropical cyclones, storm-surge models, and probabilistic sea-level rise projections to assess flood hazard associated with changing storm characteristics and sea-level rise in New York City from the pre-industrial era to 2300. Compensation between increased storm intensity and offshore shifts in storm tracks causes minimal change in modeled storm-surge heights through 2300. However, projected sea-level rise leads to large increases in future overall flood heights associated with tropical cyclones in New York City. Consequently, flood height return periods that were ~500 years during pre-industrial era have fallen to ~25 years at present, and are projected to fall to ~5 years within the next three decades.

\body

## Introduction

Coastal flooding poses a major risk to New York City (NYC), which has nearly 49.7 million built square meters and 400,000 people living within the 100-year floodplain (1). The coastal flood risk was illustrated in 2012, when Hurricane Sandy's storm surge of 2.8 m above the mean tidal level (MTL) at the Battery tide gauge produced an estimated $50 billion of damage to the region (2). Under a changing climate, the coastal flood risk to NYC is unknown. Flood risk depends not only on characteristics of tropical cyclones (TCs), extratropical cyclones, and their resultant storm surges, but also on rising sea levels, which combine with storm surge and tides to determine overall flood heights (2-5).

TCs can be approximated by a natural heat engine, or Carnot cycle (6), by which the climate system cools the oceans and atmosphere in the tropical zone. Given the predicted future warming of the atmosphere and surface-ocean waters (7), it is reasonable to expect that the climate system will generate more frequent or more intense TCs with different sizes and trajectories (8-17). However, the magnitude of changes in such TC characteristics is uncertain (3, 15-20). For NYC, the instrumental record of impacts from TC activity is too short to allow for either an accurate analysis of previous trends or to produce reliable predictions of future TC behavior. We can, however, gain insights into evolving coastal risk using an approach that involves the downscaling of state-of-the-art global climate models (GCMs) and generation of large numbers of synthetic TCs consistent with various plausible climate scenarios (3, 4, 17).

Relative sea levels will continue to rise over the next several centuries, though the magnitude of rise is uncertain (15, 21-23). The Intergovernmental Panel on Climate Change's (IPCC) Fifth

Assessment Report (AR5) projected a 'likely' (> 66% probability) global-mean SLR of 52 – 98 cm by 2100 relative to 1986-2005 in a high-emissions future [Representative Concentration Pathway (RCP) 8.5 scenario (24)], and indicated a global-mean SLR of 1 to >3 m by 2300 with medium confidence (15). But, AR5 projections of SLR are limited by uncertainties surrounding the response of the Greenland and Antarctic ice sheets (23). AR5 projected a likely contribution of the Antarctic ice sheet (AIS) of -8 – 15 cm under RCP8.5 by 2100, but a coupled ice sheet and climate dynamics model that includes marine-ice sheet instability, ice-shelf hydrofracturing, and marine ice-cliff collapse mechanisms suggests that the AIS could contribute more than 1 m by 2100, and more than 10 m by 2300, under RCP8.5 (25-27).

We assess NYC's coastal flood risk over the next three centuries based on a combination of synthetic TCs, storm-surge models, and probabilistic SLR projections (21). The estimated flood risk does not account for the influence of the tidal cycle. Although TC and SLR projections out to 2300 have less confidence, we use them to illustrate the possible evolution of flood risk in NYC beyond the end of the current century.

## Changing Storm Characteristics

We downscaled RCP8.5 simulations from three Coupled Model Intercomparison Project Phase 5 [CMIP5; (28)] models [Max-Planck-Institute Earth System Model (MPI), Coupled Climate System Model 4.0 (CCSM4), and Institut Pierre Simon Laplace Earth System Model (IPSL)] to compare storm-surge heights from the modern period (1970-2005; ~5000 storms for each model) with two future time periods (2010 – 2100 for all models and 2010 – 2300 for the IPSL model; ~12,000 storms per century for each model). These three models (henceforth 'core models') were also used in Ref. (4); thus, we can provide a pre-industrial context for results presented here. We also consider changes to TC characteristics, including trajectories and wind speeds, for storms downscaled from four additional models (HadGEM, GFDL, MRI, and MIROC; henceforth 'additional models') that include the necessary output to generate synthetic storms in future simulations (Supporting Information).

We first consider storm surge alone, which neglects the contribution of SLR to flood heights. Storm-surge return periods at the Battery tide gauge in NYC reveal either little change (CCSM4, IPSL to 2100), or slightly increased return periods (MPI, IPSL to 2300) between modern and future time periods (Fig. 1A-D). For example, the 1000-year storm surge in the IPSL model decreases from 1.8 m during 1970-2005 to 1.6 m during 2010-2300. This result differs from some previous studies of New York storm surge using CMIP3 models, which show a significant decrease of storm-surge return periods over the 21$^{st}$ century, mainly because of an increase of storm frequency and/or intensity (3, 17). In our simulations, changes to storm frequency for NYC are minimal in the future.

Principal component analysis (PCA) shows that modern and future storm surges are strongly impacted by TC radius of maximum wind (RMW) values, similar to pre-industrial era results [850 – 1800; (4)]. Level amplification factors (LAFs) of modern return periods of RMW for the CCSM4 and IPSL models suggest larger RMW values in the future (Fig. S1). An increase in future RMW values was previously suggested by Ref. (29). Larger RMW values may lead to higher wind speeds at fixed points from the storm center, which may lead to larger storm surges.

Variations in the maximum wind speed and minimum pressure of TCs from our core models also would tend to decrease storm-surge return periods. Maximum wind speeds increase (Fig.

S1) and minimum storm pressures decrease (Fig. S2) between the modern and future time periods, indicating increases in future TC intensity. For example, nearly all of the LAF values calculated for maximum wind speed in the core models were greater than 1 (Fig. S1d), indicating that future maximum wind speeds consistently exceed modern maximum wind speeds for specific return periods. Thus, consistent with previous studies (3, 9, 10, 13), our results indicate increased intensity of future TCs.

We suggest that changing TC tracks exert an important influence on future storm-surge heights in NYC (Fig. 2). In the core models, tracks move offshore between 1980-2000 (during the modern era) and 2080-2100 (during the future era). This is also true for tracks from the IPSL model in 2280-2300. The largest increase in track density (~0.025) occurs offshore between ~38– 41 °N and ~69 – 74°W; the Battery tide gauge is located at 40.7 °N, 74.015 °W. Four further metrics support the shift in TC track densities (Figs. S3-S5): 1) annual mean maximum TC wind speeds on-site at the Battery tide gauge decrease from the modern to future time period across two out of three of our core models; 2) TC winds become more westerly with time at the Battery in all core models; 3) the minimum distance between TC centers and the Battery increases over time in the time series extended to 2300 from the IPSL model; and 4) return periods of overall maximum wind speeds at the Battery (Fig. S7) show minimal changes between the modern and future time periods, suggesting a compensation between shifting tracks and increasing storm intensity in future simulations.

Projections from the four additional models are generally consistent with those from the core models. For example, the additional models also show an increase in the density of offshore tracks near NYC in 2080-2100 compared to 1980-2000, with the largest increases in densities occurring between ~39 – 42 °N, and ~67 – 72 °W (Fig. S6a). Differences in return periods of overall maximum wind speeds at the Battery between the modern and future time period are minimal in the additional models, further supporting compensation between shifting TC tracks and increasing TC intensities in the future.

The changing TC trajectories are consistent with findings from other studies of North Atlantic storms (30-34) completed using a diverse set of methodologies, including statistical models, stalagmite chronology, global best track data and reanalysis data, and overwash deposits (30-33). Further, Ref. (34) noted a poleward shift in the tracks of 21$^{st}$ century extratropical cyclones simulated from CMIP5 models, and indicated that changes to storm location and intensity likely combine to impact future surge events at the Battery, similar to our finding for TCs.

Changing patterns of sea-level pressure (SLP) for the core models favor an eastward shift in TC tracks, away from NYC (Fig. 3). Monthly mean SLP differences between the latter portions of the modern (1980-2000) and future (2080-2100) time periods during the months of August and September indicate future SLPs that are slightly higher (~300 Pa) over the Atlantic coast of the United States, and slightly lower (~200 Pa) over the North Atlantic in the future (Fig. 3a). These pressure differences intensify by the end of the 23$^{rd}$ century in the IPSL model (Fig. 3b).

## Changing Flood Heights

We define flood height at the Battery tide gauge, NYC as the sum of storm surge and SLR. We treat storm surge and SLR as independent and linearly additive; nonlinear interactions of storm surge and SLR are expected to be small at the Battery (3, 17, 35). We do not consider the effects of changes in tidal amplitude (see Methods).

To estimate the effect of SLR on flood heights in NYC in 2100 and 2300, we combined the peak storm-surge height for each synthetic storm from the core models with samples of projected SLR for 2080-2100 and 2280-2300 (Fig. S8). For both RCP4.5 and 8.5, we consider two future SLR probability distributions. First, we employ probabilistic representations of ice sheet mass loss, glacier mass loss, global mean thermal expansion, regional ocean dynamics, land water storage, and non-climatic background processes from Ref. (21), and extend those projections to 2300. Static-equilibrium fingerprints are used to translate changes in ice masses to local relative SLR. Second, we replace the AIS projections of Ref. (21) with a small ensemble generated by Ref. (26), incorporating marine-ice sheet instability, ice-cliff collapse, and ice-shelf hydrofracturing mechanisms [Fig. 4; (27)].

Relative SLR at NYC is likely to be greater than the global mean, due primarily to the combined effects of glacial isostatic adjustment and the static-equilibrium fingerprint of AIS mass changes (21, 36). Under RCP8.5, relative SLR for NYC will very likely ($P=0.90$) be 0.55 – 1.4 m (median of 0.96 m) between 2010 and 2100 and 1.5 – 5.7 m (median of 3.2 m) between 2000 and 2300. Our projections increase to 0.88 – 2.5 m (median of 1.5 m) and 10.7 – 15.7 m (median of 12.7 m) for 2100 and 2300, respectively, for the enhanced AIS input scenario (Fig. 4).

SLR causes future flood height distributions at 2080-2100 and 2280-2300 to be significantly greater than modern flood height distributions at the Battery tide gauge ($P > 0.99$ for all models and SLR projections; Fig. 5). Mean future (2080-2100) flood heights are 0.7 - 1.4 m greater than modern mean flood heights (Fig. 5A-C). For the IPSL model (Fig. 5D), mean 2280-2300 flood heights are 2.4 – 12.6 m greater than modern mean flood heights.

The changing return periods of flood heights for each of the three models for all SLR scenarios indicate the increasing risk of coastal flooding for NYC (Fig. 6). Ref. (4) found that, during the pre-industrial period (850-1800), the average 500-year return period flood height across models was approximately 2.25 m MTL at the Battery. Using a pre-industrial era baseline for sea level, the 500-year flood height increases to between 3.3 – 3.7 m MTL in all core models (Fig. 6 A-D) during the modern period (1970-2005). For simulations from 2080-2100, the mean 500-year flood height relative to the pre-industrial baseline sea level is 4.0 – 5.1 m MTL (Fig. 6 A-C). Mean 500-year flood heights for the period 2280-2300 reflect the large uncertainty in SLR projections, with flood height values ranging from 5.0 m in the RCP4.5 scenario to 15.4 m for the RCP8.5 scenario using the enhanced AIS input (26), relative to the pre-industrial baseline sea level.

The return period of the 2.25 m flood height decreases dramatically over time. The 2.25 m flood height has a return period of ~500 years during the pre-industrial era, which decreases to less than ~25 years during the modern period. In 95% of simulations, the return period of such a flood decreases to ~5 years between 2030 and 2045 (Table S1).

Increases in future NYC flood heights have also been found in a number of previous studies (17, 20, 34). However, our inclusion of SLR scenarios that incorporate large contributions to SLR and overall flood heights from the AIS results in greater increases in flood heights at the Battery by the end of the 21$^{st}$ century than earlier studies. Although there is deep uncertainty in the contributions of the AIS to SLR, the potential for large contributions should not be neglected in risk assessment.

## Discussion and Conclusions

We downscaled RCP8.5 simulations of three CMIP5 models to examine storm-surge heights and TC characteristics. There is minimal change or slightly increased storm-surge return periods (i.e., reduced risk) at the Battery tide gauge between modern and future time periods. Although there is a tendency for the strongest storms to strengthen with warming, storm tracks shift offshore at the latitude of NYC, offsetting the effects of increased storm intensity on storm surges at the Battery. However, stronger storms with shifted tracks could lead to more direct or severe TC impacts in other coastal regions, such as New England or northwestern Europe—an issue that merits further study. We note that a climate with stronger storms opens the possibility of a rare and very damaging event to the NYC region, even if such storms are typically routed away from the area.

As with any study involving GCMs, our results are subject to limitations related to the accuracy of modeled atmospheric-ocean dynamics, which drive the behavior and tracks of downscaled TCs. Of particular relevance is the limited skill of CMIP5 models in simulating the Atlantic meridional overturning circulation (AMOC) and Arctic sea ice loss (37, 38). Although CMIP5 models generally project a weakening of the AMOC by 2100, the degree of weakening varies greatly across individual models (37). In addition, although GCMs continue to improve their representation of Arctic sea ice loss, most CMIP5 models still underestimate observed trends (38). Biases in projections of both phenomena may impact TC trajectories.

In particular, underestimation of AMOC weakening may lead to an underestimation of the anomalously cool sea-surface temperatures that have been observed south of Greenland in the North Atlantic (39). Together with difficulty projecting Arctic sea ice loss, this limitation may limit skill in modeling high-pressure patterns in the North Atlantic (e.g., 41-45). Such high-pressure patterns could block TC paths to the north, directing more TC tracks towards NYC (similar to the path that Hurricane Sandy took in 2012). Moreover, a southerly bias in projections of the Gulf Stream path due to an underestimation of AMOC weakening could also reduce the number of TC tracks reaching NYC (40).

Beyond the limitations of GCMs, it should also be noted that, like many previous studies (3, 4, 17), we do not consider the extratropical transition of storms as they move to higher latitudes. The extratropical transition of TCs that impact the northeastern U.S. is not uncommon (46) and can result in storms such as Hurricane Sandy (2012), which generated devastating surges in NYC as a post-tropical cyclone. Sediment records of coastal flooding near NYC support the idea that the frequency of major flood events may be underestimated in GCM studies (17).

Regardless of TC characteristics, SLR will greatly increase future flood risk for NYC, where SLR is projected to be more rapid than the global mean (21, 36). Sea levels are expected to continue rising for at least the next several centuries, more than offsetting any potential decreases in storm-surge heights (15, 17, 21-23).

# Methods

## Study Area

We focus our study at the Battery in NYC. Storm-surge heights and flood heights are given relative to MTL, or the arithmetic mean of mean low water and mean high water at the Battery tide gauge over the present National Tidal Datum Epoch (1983-2001). The National Oceanic and Atmospheric Administration (NOAA) tide gauge network for the Battery tide gauge indicates that 1) the present great diurnal range (GT--height difference between mean higher high water and mean lower low water) is 1.54 m 2) the present mean tidal range is 1.38 m, and 3) the height difference between spring and neap tides is typically ~0.5 m.

## Synthetic Tropical Cyclone Datasets

The downscaling method described in Refs. (47) and (48) is applied here to the core models for the CMIP5 RCP8.5 experiments. In this downscaling method, TC tracks are approximated with a beta-and-advection model, which uses synthetic wind time series at 850 and 250 hPa to determine storm motion (48). Methods applied to simulations of future TCs are the same as those described in the historical analysis presented in Ref. (4), including the deterministic calculation of RMW values using the Coupled Hurricane Intensity Prediction System, or CHIPS model (48). Our analysis applies the basin mean value of storms' outer radius to all storms, which may induce a low bias in the estimated storm-surge distributions (17, 49-51; see Supporting Information for further explanation).

Pre-industrial era TC and storm-surge datasets referred to here are the same as the pre-anthropogenic datasets described in Ref. (4), and the modern era surge and TC datasets referred to here are the same as the anthropogenic datasets used in Ref. (4). Note that pre-industrial and modern datasets contain ~5000 storms for each model. For reliable statistical analysis of future storm-surge heights in this region, we use datasets that include more than 12,000 storms per century with centers that pass within 250 km of the Battery. Overall event frequency is calculated from the ratio of the total number of simulated TC events to the total number seeded.

## Storm-Surge Modeling

As in Ref. (4), we apply the Advanced Circulation (ADCIRC) model (52) to simulate the storm surges induced by all synthetic storms. ADCIRC is a finite-element hydrodynamic model that has been successfully used to simulate and forecast storm-surge events for coastal regions (e.g., 53, 54). The numerical grid and modeling specifics used here were developed by Ref. (3) and used in Refs. (4) and (17).

Consistent with previous work, storm surge is defined here as the anomalous rise of water above MTL, and flood height is defined as the sum of storm surge and change in relative sea level (4, 17). Storm-surge height is primarily determined by a TC's wind patterns and track, coastal geography, and, to some extent, the reduced atmospheric pressure associated with a storm. Storm-surge heights are thus highly dependent upon the TCs that generate them, as they are significantly affected by TC characteristics, including intensity, size, duration, and location (3, 4, 13). The effect of changes in wave set-up for the region is expected to be small, and is not included in our storm-surge calculations.

Additionally, although there has been some work indicating that interactions between storm surge and tide are not strictly linear (3), flood heights are calculated here relative to MTL, and a full tidal cycle is not accounted for in our discussion of changing flood heights from the pre-industrial era to the future. It is possible that tides may evolve in a changing climate (55). Although recent work suggests that changing bathymetric depth has little influence at the

Battery, evidence does support a strong, approximately linear relationship between GT and the bathymetric depth of Long Island Sound (56). Further, tides can be very important in determining overall flooding, influencing the highest water levels reached during a storm-surge event (2, 56). The influence of tides upon overall flood heights varies greatly from storm to storm (Supporting Information), but is likely to be most significant with large or slow-moving TCs, such as Hurricane Sandy. Tidal contributions to overall flood heights are well documented for major historical TCs impacting NYC, including the 1938 New England Hurricane (40% tidal contribution to the overall 1.57m storm tide), Hurricane Donna (1960; 29% tidal contribution to the overall 2.30 m storm tide), Hurricane Gloria (1985; 12% tidal decrease of the 1.9 m surge to a 1.7 m storm tide), and Hurricane Sandy (19% tidal contribution to the overall 3.47 m storm tide; 2). Thus, our decision to make our calculations using the MTL tidal datum constitutes an important caveat for this work.

We use a linear combination of storm surge and sea level (from proxy records and SLR projections) to generate flood heights at the Battery. To view the results presented here in the context of the historical analysis presented in Ref. (4), future sea level from SLR projections for each year was adjusted to be relative to a pre-industrial era baseline (4, 57).

Ref. (3) shows that, especially for SLR amounts of about 1.8 m or less, the non-linear effect of SLR on storm-surge heights at the Battery is very small; Ref. (35) also demonstrates similar flood levels at the Battery for both static and dynamically modeled floods of up to about 5.8 m. However, while such a linear combination of surge and SLR may provide a close approximation, it may also result in a slight underestimation of final flood heights (58, 59), which could cause some of the flood heights presented here to be somewhat lower than what we would expect if SLR were fully integrated into ADCIRC.

## Future Sea-Level Rise Projections

For the future mean sea levels upon which simulated storm-surge events occur, we use 10,000 Monte Carlo (MC) samples of projected sea level at the Battery for both the RCP4.5 and RCP8.5 scenarios, based upon the framework of Ref. (21). SLR projections are developed based on the CMIP5 archive for thermal expansion and ocean dynamics, surface-mass balance modeling for glacier melt, a combination of the AR5 expert assessment and the expert elicitation of Ref. (60) for ice sheet contributions, semi-empirical modeling of land water storage, statistical modeling of non-climatic local sea-level change, and geophysical modeling of gravitational, elastic and rotational effects on local sea level (21). We also generated a set of projections in which we replaced the west and east AIS projections of Ref. (21) with random samples from the 5-20 m Pliocene, non-bias-adjusted RCP4.5 and RCP8.5 ensembles of Ref. (26). It should be noted that Ref. (26) was not attempting to construct a probability distribution of future AIS changes; its ensemble of 29 members can be viewed neither as spanning the full range of possibilities with minimal gaps nor as having a defined probability associated with each member. Thus, the distribution of this second set of projections may be viewed as a frequency distribution from a modeled set of possible futures, but not as a probability distribution of future SLR (27).

The projections used here differ from those of Refs. (21) and (26) in two important ways. First, the projections are extended to 2300, while those of Ref. (21) ended in 2200. For the ocean dynamic and thermal expansion components, we achieve this extension by continuing to use

GCM projections that extend to 2300. For glacier projections, we do the same using surface-mass balance projections driven by GCM projections extending to 2300. For the Greenland ice sheet and for AIS in the ensemble consistent with AR5, we continue the linear growth of ice sheet melt rates beyond 2200. Second, for the ensemble employing the AIS projections (26), we employ the full time series of projections; only 2100 and 2500 values are reported in Ref. (26).

Pre-industrial and modern relative sea level datasets used in this study to calculate flood heights during these time periods are the same as those described in Ref. (4), developed from relative sea level reconstructions in southern New Jersey (57).

## Statistics

Distributions of TC characteristics used to calculate return periods and LAFs (Fig. S1) are produced by generating 25,000 bootstrap samples of ~5000 events for both the modern and future time periods (61). Similarly, distributions of storm surges used to calculate mean and 95% confidence intervals of storm-surge return periods (Fig. 1) are produced by generating 100,000 bootstrap samples of ~5000 storm-surge events for both the modern and future time periods. Additionally, distributions of flood heights used to calculate return periods over short time periods (2080-2100 and 2280-2300; Fig. 6) are produced by generating 100,000 bootstrap samples of 2835 storm-surge events from the time period of interest in the original storm-surge data set, and combining each bootstrap sample with a randomly selected SLR time series from the MC samples.

We use PCA to analyze variations and patterns between TC characteristics and storm surge. In addition, we examine LAFs to compare modern and future return periods. We define the LAF of a variable as the ratio of the variable's future value to its modern value for a given return period; it indicates the degree to which the variable increases or decreases in the future compared to the modern era.

## Data Availability

Data used here are publicly available from the Earth System Grid Federation website, (https://www.earthsystemgrid.org/home.html). SLR projections were generated using ProjectSL (https://github.com/bobkopp/ProjectSL) and LocalizeSL (https://github.com/bobkopp/LocalizeSL). Researchers interested in downscaled fields may contact co-author KAE or AJG via e-mail with their request.

## Acknowledgments

The authors acknowledge funding for this study from NOAA Grants # 424-18 45GZ and # NA11OAR4310101, National Science Foundation (NSF) Grants OCE 1458904, EAR 1520683, and EAR Postdoctoral Fellowship 1625150, the Community Foundation of New Jersey, and David and Arleen McGlade.

We acknowledge the World Climate Research Programme's Working Group on Coupled Modeling, which is responsible for CMIP, and we thank the MPI, CCSM4, IPSL, HadGEM, GFDL, MRI, and MIROC climate modeling groups for producing and making available their model output. For CMIP the U.S. Department of Energy's Program for Climate Model Diagnosis and

Intercomparison provides coordinating support and led development of software infrastructure in partnership with the Global Organization for Earth System Science Portals.

We appreciate technical assistance from Sonya Miller, and advice, comments, and input from David Titley, Raymond Najjar, and Gregory Garner.

This paper is a contribution to PALSEA2 (Palaeo-Constraints on Sea-Level Rise) and International Geoscience Programme (IGCP) Project 639, “Sea Level Change from Minutes to Millennia.” This is Earth Observatory Publication contribution 210.

# References

1. NYC Special Initiative for Rebuilding and Resiliency, *A Stronger, more Resilient New York* (PlaNYC, New York City, 2013).

2. Kemp AC, Horton BP (2013) Contribution of relative sea-level rise to historical hurricane flooding in New York City. *J Qua Sci* 28: 537-541.

3. Lin N, Emanuel KA, Oppenheimer M, Vanmarcke, E (2012) Physically based assessment of hurricane surge threat under climate change. *Nat Clim Change* 2: 462-467.

4. Reed AJ, *et al.* (2015) Increased threat of tropical cyclones and coastal flooding to New York City during the anthropogenic era. *Proc Natl Acad Sci* 112: 12610-12615.

5. Little CM, *et al.* (2015) Joint projections of US East Coast sea level and storm surge. *Nat Clim Change* 5: 1114-1120.

6. Emanuel KA (1987), The dependence of hurricane intensity on climate. *Nature* 326: 483-485.

7. IPCC (2014) Climate Change 2014: Synthesis Report. Contribution of Working Groups I, II, and III to the fifth Assessment Report of the Intergovernmental Panel on Climate Change [Core Writing Team, RK Pachauri and LA Meyer (eds.)]. IPCC, Geneva, Switzerland, 151 pp.

8. Villarini G, Vecchi GA (2013) Projected increases in North Atlantic tropical cyclone intensity from CMIP5 models. *J Clim* 26: 3231-3240.

9. Emanuel KA (2013) Downscaling CMIP5 climate models shows increased tropical cyclone activity over the 21st century. *Proc Nat Acad Sci* 110: 12219-12224.

10. Knutson TR, *et al.* (2015) Global projections of intense tropical cyclone activity for the late twenty-first century from dynamical downscaling of CMIP5/RCP4.5 scenarios. *J Clim* 28: 7203-7224.

11. Kossin JP, Camargo SJ, Sitkowski M. (2010) Climate modulation of North Atlantic hurricane tracks. *J Clim* 23: 3057-3076.

12. Woodruff JD, Irish J, Camargo S (2013) Coastal flooding by tropical cyclones and sea-level rise. *Nature* 504: 44-52.

13. Lin N, Emanuel KA, Smith JA, Vanmarcke E. (2010) Risk assessment of hurricane storm surge for New York City. *J Geophys Res-Atmos* 115: D18121.

14. Kossin JP (2017) Hurricane intensification along United States coast suppressed during active hurricane periods. *Nature* 541: 390-393.

15. Intergovernmental Panel on Climate Change (IPCC), (2013) “Climate Change 2013: The Physical Science Basis. Contribution of Working Group I to the Fifth Assessment Report of the Intergovernmental Panel on Climate Change.” eds Stocker TF, et al. (Cambridge University Press, Cambridge, United Kingdom and New York, NY, USA).

16. Knutson TR, *et al.* (2010) Tropical cyclones and climate change. *Nat Geosci* 3: 157-163.

17. Lin N, Kopp RE, Horton BP, Donnelly JP (2016) Hurricane Sandy’s flood frequency increasing from year 1800 to 2100. *Proc Natl Acad Sci* 113: 12071-12075.

18. Reed AJ, Mann ME, Emanuel KA, Titley DW (2015) An analysis of long-term relationships among count statistics and metrics of synthetic tropical cyclones downscaled from CMIP5 models. *J Geophys Res Atm* 120: 7506-7519.

19. Walsh K (2008) The ability of climate models to generate tropical cyclones: implications for prediction. *Climate Change Research Progress,* ed L. Peretz (Nova Publishers), pp 313-329.

20. Horton R, Little C, Gornitz V, Bader DA, Oppenheimer M (2015) New York City Panel on Climate Change 2015 Report: Sea level rise and coastal storms. *Ann New York Acad Sci* 1336: 36-44.

21. Kopp RE, *et al.* (2014) Probabilistic 21st and 22nd century sea-level projections at a global network of tide-gauge sites. *Earth’s Future* 2: 383-406.

22. Levermann A, *et al.* (2013) The multimillennial sea-level commitment of global warming. *Proc Nat Acad Sci* 110: 13745-13750.

23. Horton BP, Rahmstorf S, Engelhart SE, Kemp AC (2014) Expert assessment of sea-level rise by AD 2100 and AD 2300. *Quat Sci Rev* 84: 1-6.

24. Riahi K, *et al.* (2011) RCP 8.5—A scenario of comparatively high greenhouse gas emissions. *Climatic Change* 109: 33-57.

25. Pollard D, DeConto RM, Alley RB (2015) Potential Antarctic Ice Sheet retreat driven by hydrofracturing and ice cliff failure. *Earth Plan Sci Lett* 412: 112-121.

26. DeConto RM, Pollard D (2016) Antarctica's Contribution to Past and Future Sea-Level Rise. *Nature* 531: 591-597.

27. Kopp RE, *et al.* (2017) Implications of Antarctic ice-cliff collapse and ice-shelf hydrofracturing mechanisms for sea-level projections. *ArXiv e-prints.* eprint: 1704.05597

28. Taylor KE, Stouffer RJ, Meehl GA (2012) An overview of CMIP5 and the experiment design. *Bull Am Meteorol Soc* 93:485-498.

29. Mudd L, Wang Y, Letchford C, Rosowsky D (2014) Hurricane wind hazard assessment for a rapidly warming climate scenario. *J.Wind Eng. And Ind.Aerodyn.* 133: 242-249.

30. Hall T, Yonekura E (2013) North American tropical cyclone landfall and SST: A statistical model study. *J Clim* 26: 8422-8439.

31. Baldini LM, *et al.* (2016) Persistent northward North Atlantic tropical cyclone track migration over the past five centuries. *Nature: Sci Reports* 6: 37522.

32. Kossin JP, Emanuel KA, Vecchi GA (2014) The poleward migration of the location of tropical cyclone maximum intensity. *Nature.* 509: 349-352.

33. Van Hengstum PJ et al., (2015) The intertropical convergence zone modulates intense hurricane strikes on the western North Atlantic margin. *Sci.Reports*, 6: 21728.

34. Roberts K, Colle B, Korfe N (2016) Impact of simulated 21st century changes in extratropical cyclones on coastal flooding at The Battery, New York City. *J Appl Meteor Climatol*

35. Orton P, *et al.* (2015) New York City Panel on Climate Change 2015 Report Chapter 4: Dynamic Coastal Flood Modeling. *Ann NY Acad Sci* 1336: 56-66.

36. Kopp RE, Hay CC, Little CM, Mitrovica JX (2015) Geographic variability of sea-level change. *Current Climate Change Reports* 1: 192-204.

37. Cheng W, Chiang JCH, Zhang D (2013) Atlantic Meridional Overturning Circulation (AMOC) in CMIP5 Models: RCP and Historical Simulations. *J. Clim.* 26: 7187-7197.

38. Stroeve JC et al. (2012) Trends in Arctic sea ice extent from CMIP5, CMIP3 and observations. *Geophys. Res. Lett.* 39: L16502.

39. Rahmstorf S et al. (2015) Exceptional twentieth-century slowdown in Atlantic Ocean overturning circulation. *Nat. Clim.* 5: 475-480.

40. Joyce TM, Zhang R (2010) On the Path of the Gulf Stream and the Atlantic Meridional Overturning Circulation *J Clim* 23: 3146-3154.

41. Petoukhouv V and Semenov VA (2010) A link between reduced Barents-Kara sea ice and cold winter extremes over northern continents. *J. Geophys. Res. Atm.* 115: D21111.

42. Francis JA and Vavrus SJ (2012) Evidence linking Arctic amplification to extreme weather in mid-latitudes. *Geophys. Res. Lett.* 39: L06801.

43. Liu JP, Curry JA, Wang HJ, Song MR, and Horton RM (2012) Impact of declining Arctic sea ice on winter snowfall. *Proc. Nat. Acad. Sci.* 109: 4074-4079.

44. Jaiser R, Dethloff K, Handorf D, Rinke A, Cohen J (2012) Impact of sea ice cover change on the Northern Hemisphere atmospheric winter circulation. *Tellus A.* 64.

45. Haarsma RJ, Selten FM, Drijfhout, SS (2015) Decelerating Atlantic meridional overturning circulation main cause of future west European summer atmospheric circulation changes. *Env. Res. Lett.,* 10: 094007.

46. Hart RE, Evans JL (2000) A Climatology of the Extratropical Transition of Atlantic Tropical Cyclones. *J Clim* 14: 546-564.

47. Emanuel KA, Ravela S, Vivant E, Risi C (2006) A statistical-deterministic approach to hurricane risk assessment. *Bull Am Meteorol Soc* 19: 299-314.

48. Emanuel KA, Sundararajan R, Williams J (2008) Hurricanes and global warming: Results from downscaling IPCC AR4 simulations. *Bull Am Meteorol Soc* 89: 347-367.

49. Lin N, Lane P, Emanuel KA, Sullivan RM, Donnelly JP (2014) Heightened hurricane surge risk in northwest Florida revealed from climatological-hydrodynamic modeling and paleorecord reconstruction. *J Geophys Res-Atmos* 119: 8606-8623.

50. Chavas D, Lin N, Emanuel KA (2015) A model for the complete radial structure of the tropical cyclone wind field. Part I: Comparison with observed structure. *J Atmos Sci* 72: 3647-3662.

51. Chavas D, Lin N (2016) A model for the complete radial structure of the tropical cyclone wind field. Part II: Wind field variability. *J Atmos Sci* 73: 3093-3113.

52. Luettich RA, Westerink JJ, Scheffner NW (1992) ADCIRC: An advanced three-dimensional circulation model for shelves, coasts, and estuaries, Report 1: Theory and methodology of ADCRIC-2DDI and ADCIRC-3DL (Tech. Rep. DRP-92-6, U.S. Army Corps of Engineers).

53. Westerink JJ, *et al.* (2008) A basin- to channel-scale unstructured grid hurricane storm surge model applied to southern Louisiana. *Mon Weather Rev* 136: 833-864.

54. Colle BA, *et al.* (2008) New York City's vulnerability to coastal flooding. *Bull Am Meteorol Soc* 89: 829–841.

55. Muller M (2011) Rapid change in semi-diurnal tides in the North Atlantic since 1980. *Geophys Res Lett* 38: L11602.

56. Kemp AC *et al.* (2017) Relative sea-level trends in New York City during the past 1500 years. *The Holocene*.

57. Kemp AC, *et al.* (2013) Sea-level change during the last 2500 years in New Jersey, USA. *Quat Sci Rev* 81: 90-104.

58. McKee Smith J, Cialone MA, Wamsley TV, McAlpin TO (2009) Potential impact of sea level rise on coastal surges in southeast Louisiana. *Ocean Eng* 37: 37-47.

59. Zhang K, Li Y, Liu H, Xu H, Shen J (2012) Comparison of three methods for estimating the sea level rise effect on storm surge flooding. *Clim Change* 118: 487-500.

60. Bamber JL, Aspinall WP (2013) An expert judgement assessment of future sea level rise from the ice sheets. *Nat Clim Change* 3: 424-427.

61. Efron B, Tibshirani RJ, *An Introduction to the Bootstrap* (Chapman and Hall, 1993).

62. E Blake ES, Kimberlain TB, Berg RJ, Cangialosi JP, Beven JL, II (2013) Tropical Cyclone Report: Hurricane Sandy (AL182012), 22-29 October 2012. National Hurricane Center.

63. Landsea CW, *et al.* (2004) A reanalysis of Hurricane Andrew's intensity. *Bull Am Meteorol Soc.*

# Figure Legends

**Figure 1:** Return Periods of storm-surge heights. Results are shown for the modern (blue) and future (red) periods for (A) the MPI model, (B) the CCSM4 model, (C) the IPSL model, and (D) the IPSL model where future simulations extend to 2300. The 95% credible interval of storm-surge events is shown in light blue for modern, and in light red for future.

**Figure 2:** Multi-model mean difference between future and modern synthetic TC track densities from the MPI, CCSM4, and IPSL models. Track densities are determined by the sum total of tracks crossing through each grid box over 20-year periods from 2080-2100 and 1980-2000, divided by the area of that grid box and the number of years (21). Here the grid box latitude-longitude scales are determined by the output resolution of the model in question.

**Figure 3:** Mean August and September SLP differences. Pressure differences (pascals) are between (A) 2080-2100 and 1980-2000 for all three models, and (B) 2280-2300 and 1980-2000 for the IPSL model. Color bars show the range of SLP differences.

**Figure 4:** Sea level projections from 2010 to 2300. Projections are calculated using RCP4.5 (yellow) and RCP8.5 (orange) projections (21), and for projections combining AIS contributions from ref. (26) with the RCP4.5 (red) and RCP8.5 (dark red) projections from ref. (21). Lines and shaded regions represent the median and the central 95% credible interval.

**Figure 5:** Normalized distributions of flood heights. Distributions are for the modern (1970-2005) and future eras for flood heights calculated using the RCP4.5 and RCP8.5 SLR projections (21), and for flood heights calculated by combining AIS contributions (26) with the RCP4.5 and RCP8.5 SLR projections (21). Results are shown for future scenarios for (A) the MPI model, (B) the CCSM4 model, (C) the IPSL model and (D) the IPSL model to 2300.

**Figure 6:** Return periods of flood heights. Results are for the modern (1970-2005) and future eras for flood heights calculated using the RCP4.5 (yellow) and RCP8.5 (orange) SLR projections (21), and for flood heights calculated by combining AIS contributions (26) with the RCP4.5 (red), and RCP8.5 (burgundy) SLR projections (21). Results are shown for future simulations for (A) the MPI model, (B) the CCSM4 model, (C) the IPSL model, and (D) the IPSL model to 2300. The gray, horizontal dotted line on each plot indicates the 500 year return period, and the black diamond on each plot indicates the 500-year flood height (2.25 m) for the pre-industrial era (4); mean and 95% credible intervals of flood heights for each return period are shown by the solid line and the shaded region between dashed lines on each plot.

# Figures

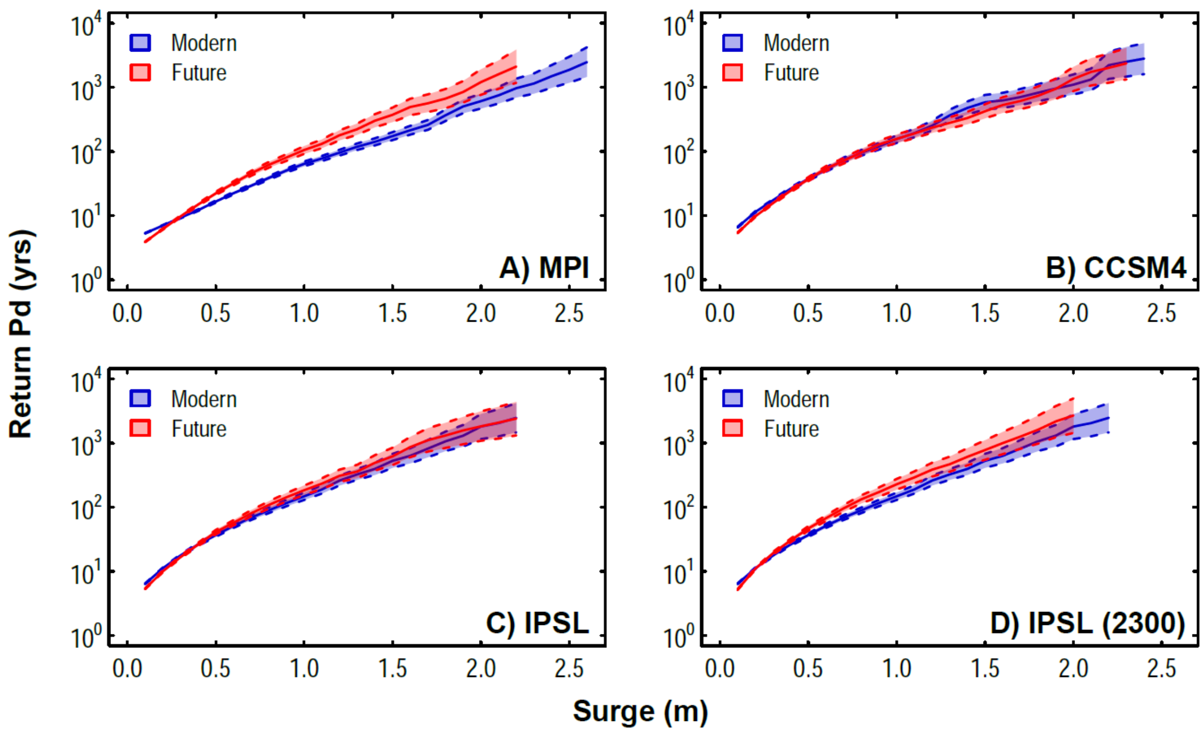


**Figure 1:** Return Periods of storm-surge heights. Results are shown for the modern (blue) and future (red) periods for (A) the MPI model, (B) the CCSM4 model, (C) the IPSL model, and (D) the IPSL model where future simulations extend to 2300. The 95% credible interval of storm-surge events is shown in light blue for modern, and in light red for future.

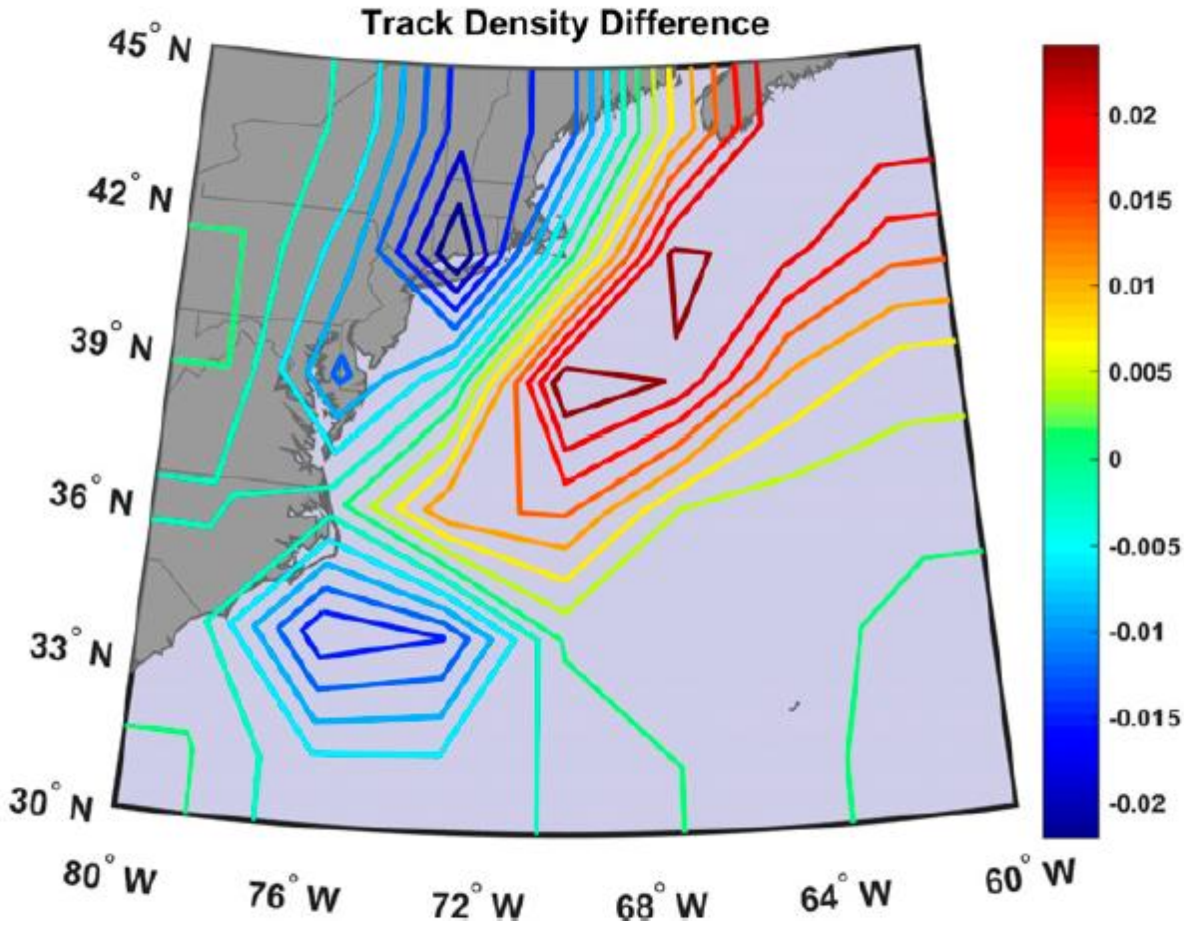


**Figure 2:** Multi-model mean difference between future and modern synthetic TC track densities from the MPI, CCSM4, and IPSL models. Track densities are determined by the sum total of tracks crossing through each grid box over 20-year periods from 2080-2100 and 1980-2000, divided by the area of that grid box and the number of years (21). Here the grid box latitude-longitude scales are determined by the output resolution of the model in question.

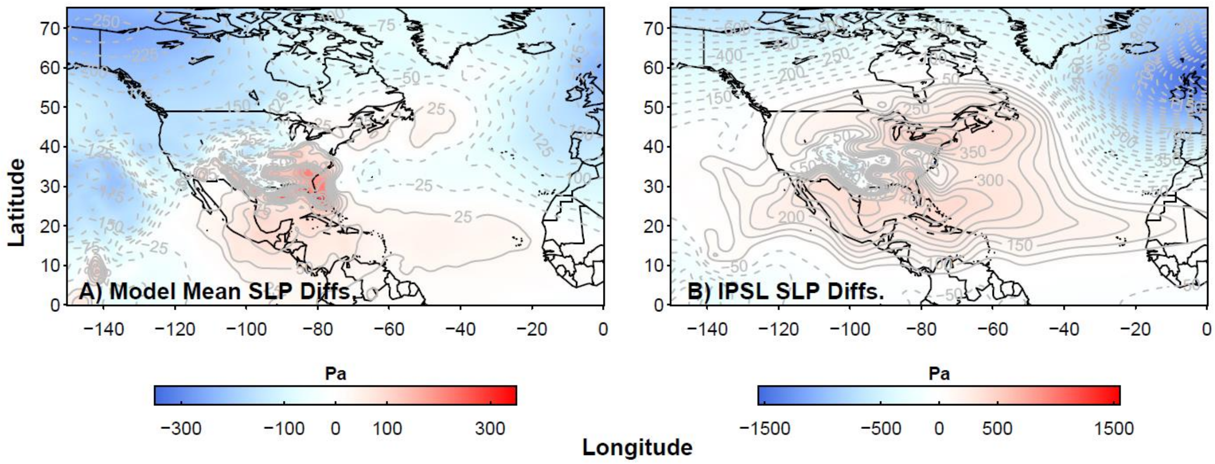


**Figure 3:** Mean August and September SLP differences. Pressure differences (pascals) are between (A) 2080-2100 and 1980-2000 for all three models, and (B) 2280-2300 and 1980-2000 for the IPSL model. Color bars show the range of SLP differences.

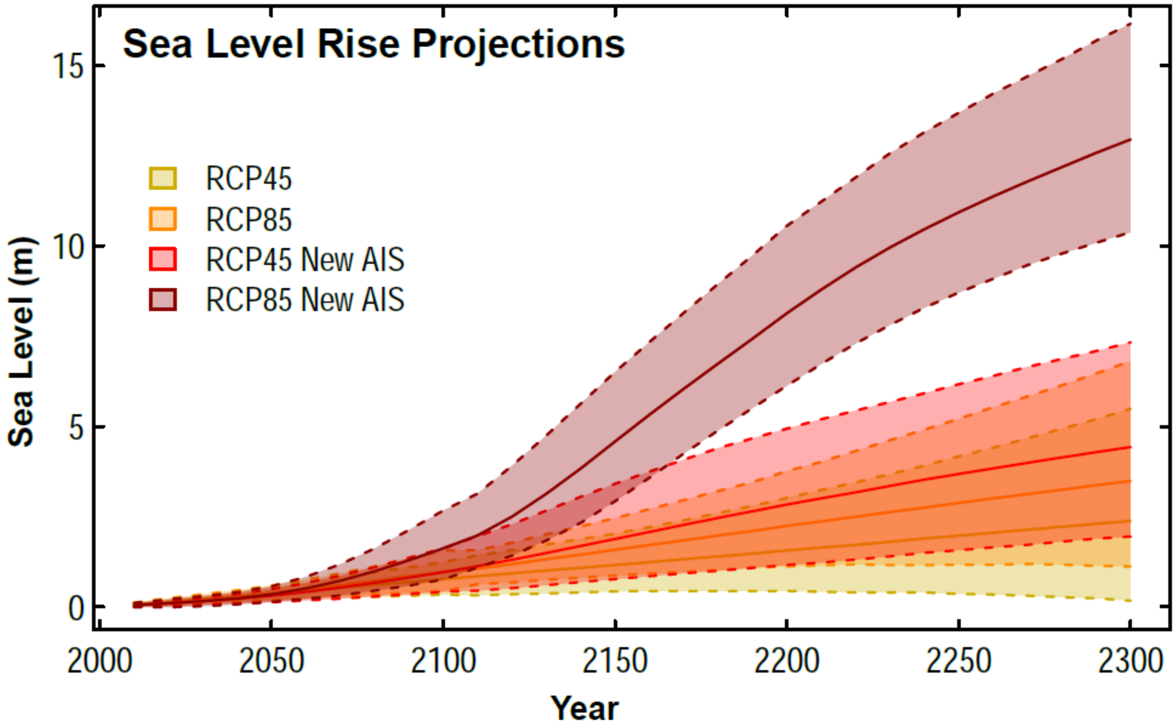


**Figure 4:** Sea level projections from 2010 to 2300. Projections are calculated using RCP4.5 (yellow) and RCP8.5 (orange) projections (21), and for projections combining AIS contributions from ref. (26) with the RCP4.5 (red) and RCP8.5 (dark red) projections from ref. (21). Lines and shaded regions represent the median and the central 95% credible interval.

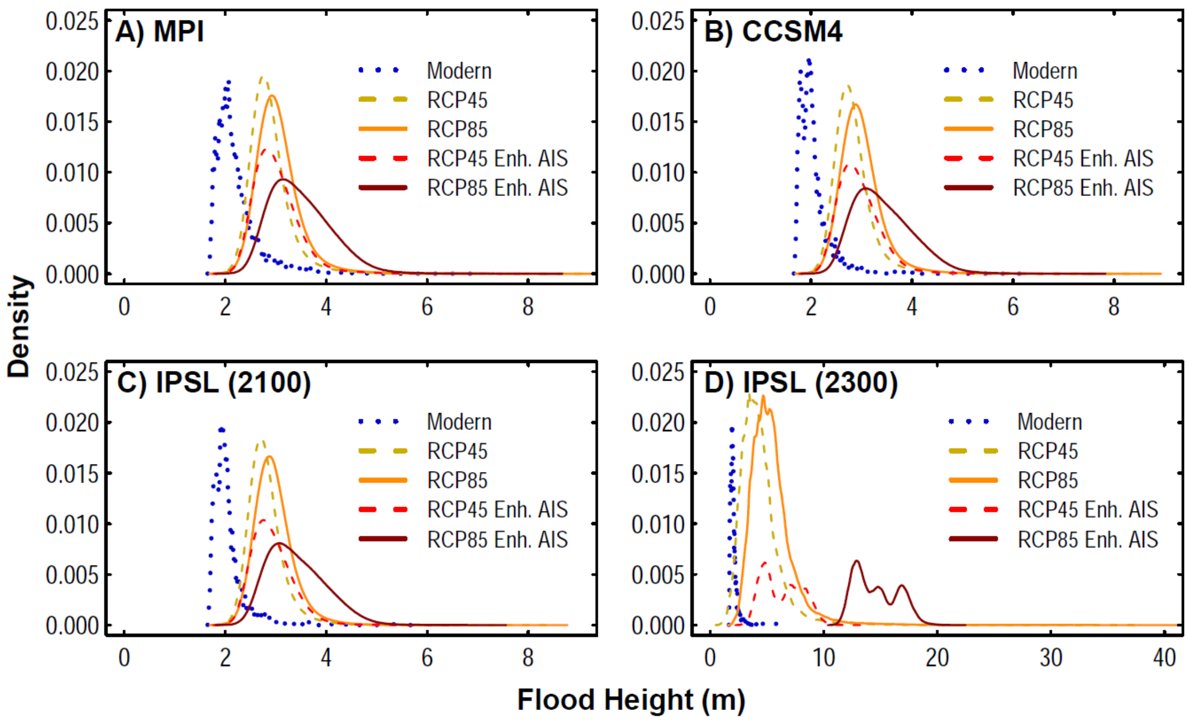


**Figure 5:** Normalized distributions of flood heights. Distributions are for the modern (1970-2005) and future eras for flood heights calculated using the RCP4.5 and RCP8.5 SLR projections (21), and for flood heights calculated by combining AIS contributions (26) with the RCP4.5 and RCP8.5 SLR projections (21). Results are shown for future scenarios for (A) the MPI model, (B) the CCSM4 model, (C) the IPSL model and (D) the IPSL model to 2300.

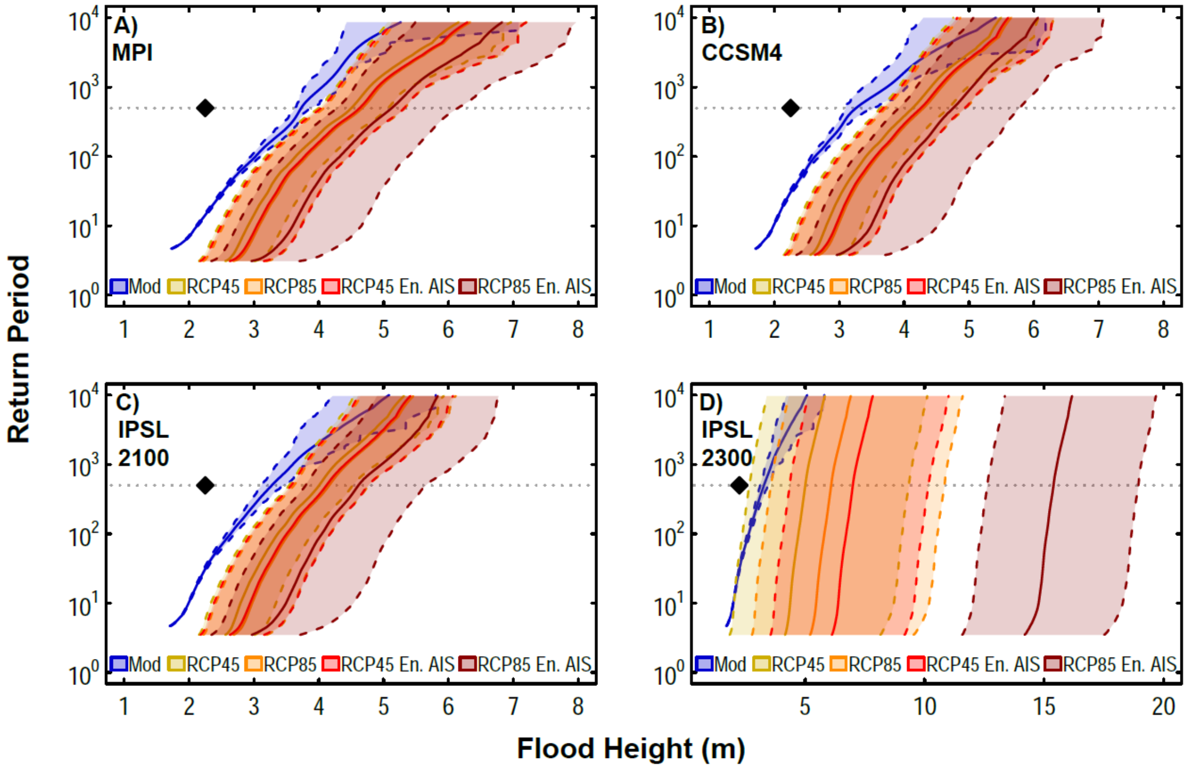


**Figure 6:** Return periods of flood heights. Results are for the modern (1970-2005) and future eras for flood heights calculated using the RCP4.5 (yellow) and RCP8.5 (orange) SLR projections (21), and for flood heights calculated by combining AIS contributions (26) with the RCP4.5 (red), and RCP8.5 (burgundy) SLR projections (21). Results are shown for future simulations for (A) the MPI model, (B) the CCSM4 model, (C) the IPSL model, and (D) the IPSL model to 2300. The gray, horizontal dotted line on each plot indicates the 500 year return period, and the black diamond on each plot indicates the 500-year flood height (2.25 m) for the pre-industrial era (4); mean and 95% credible intervals of flood heights for each return period are shown by the solid line and the shaded region between dashed lines on each plot.